

## Nodal structures of intrashell states of three-valence-electron atoms

C. G. Bao,<sup>1</sup> Xiazhou Yang,<sup>2</sup> and C. D. Lin<sup>2</sup>

<sup>1</sup>*Department of Physics, Zhongshan University, Guangzhou, 510275, People's Republic of China*

<sup>2</sup>*Department of Physics, Kansas State University, Manhattan, Kansas 66506*

(Received 26 August 1996; revised manuscript received 4 February 1997)

The nodal structures of intrashell states of a three-valence-electron atom are investigated. We expand the wave function in the body frame of the three electrons and show that the effect of symmetry such as rotation, space inversion, and permutation is to impose nodal surfaces on the components of the wave function. The equilibrium configuration is deduced to be a coplanar equilateral triangle with the core at the center and the three electrons at the vertices. Three basic modes of internal oscillations have been identified and the relative energy levels of the atom are interpreted in terms of the degrees of excitations of these basic modes. Calculations are carried out using a model of three electrons moving on the surface of a sphere. Results from this  $r$ -frozen model, as well as the limited data in the literature, are used to illustrate conclusions drawn only from the symmetry consideration alone. We thus claim that the relative energy levels of intrashell states of a three-electron atom is determined less by the detailed dynamics and interactions, but more by the inherent quantum symmetry. [S1050-2947(97)02406-2]

PACS number(s): 31.50.+w, 03.65.-w, 21.45.+v, 31.15.Hz

### I. INTRODUCTION

The properties of singly excited states in a many-electron atom are well understood in general based on the shell model. The wave function of the outermost electron is analogous to the well-known wave function of the hydrogen atom and the principal quantum number  $n$ , which is used to designate excited states, is directly a measure of the number of nodes in the radial wave function. When two electrons are simultaneously excited, the shell model picture fails. Over the past three decades a number of theoretical approaches have been developed to describe these doubly excited states. The emerged picture of doubly excited states is that the motion of the two electrons has to be treated together and that the excitation spectrum can be understood qualitatively in terms of quanta of the joint rotation and vibration of the two electrons (see [1] and references therein). Further analysis has established that these quanta are related to the nodal structure of the wave functions in some internal coordinates. Today the basic behavior of doubly excited states of atoms is fairly well understood; methods for performing accurate calculations are available and theoretical approaches are capable of explaining the ever-improving high-resolution data such as those obtained using synchrotron radiation [2,3].

One of the next challenges in basic atomic structure studies lies in the understanding of triply excited states. When compared to doubly excited states of a two-electron system, the addition of one more electron introduces three more spatial degrees of freedom and one more spin degree of freedom. By removing the three degrees of freedom describing the rotation of the whole system, there are six remaining spatial internal degrees of freedom. Thus, even without consideration of spins, we need six quantum numbers to describe a three-electron wave function, which in turn provides the full description of the system.

The complexities and the large degrees of freedom that are needed to describe a three-electron atom guarantee that full understanding will come out only slowly. While experi-

mental data from synchrotron radiation laboratories for Li atoms are beginning to emerge, only a very small subset of triply excited states have been explored so far [4–6]. Similarly, a limited number of individual states of a three-electron system have been calculated by the conventional approaches [7–11], but the nature and the systematical behaviors of triply excited states still have not been investigated. Due to the high dimensionality of the wave functions, the extraction of meaningful physical parameters or approximate quantum numbers that characterize triply excited states is a formidable challenge and perhaps is even more difficult than performing the actual numerical calculation for individual states. On the other hand, without a set of different approximate quantum numbers to describe the internal modes or the relative motions of the three electrons, we cannot claim to have understanding of the triply excited states. Alternative approaches based on hyperspherical coordinates may provide some hope for the analysis of these states [12–14], but the methods are not fully developed yet and even then the identification of meaningful physical parameters is nontrivial.

In this paper we study the effect of symmetry on the intrashell states of three-valence-electron atomic systems. In particular, we examine the nodal structures of the wave functions when the three electrons are at the same distances from the nucleus. We show that nodal surfaces are imposed on the wave functions due to the overall symmetry of the states and the existence of nodal surfaces in turn determines most importantly the relative energy levels of intrashell states.

The rest of this article is arranged as follows. In Sec. II we first describe the decomposition of the wave function on the body frame of the three electrons. For each  $L$ ,  $S$ , and parity  $\pi$ , we then address the condition of symmetry on the rotational component wave functions, in particular, in terms of the existence of nodal surfaces. These types of nodal surfaces occur when the three electrons have special symmetry, such as forming an equilateral triangle, an isosceles triangle, or a coplanar equilateral triangle. Modes of small “vibrations”

from these equilibrium configurations are then identified. Since any nodal surfaces imply higher kinetic energies, the low-lying states of a three-electron atom will try to avoid exciting those rotational components that have inherent nodal surfaces. For the higher states, additional nodal surfaces are excited. By analyzing the nature of nodal surfaces for all the rotational components for all the  $L$ ,  $S$ , and  $\pi$  symmetries, the relative energy levels of a three-electron atom can be more or less deduced (Sec. III). In Sec. IV we used the wave functions obtained from the model calculations where the three electrons are assumed to lie on the surface of a sphere to illustrate that indeed the qualitative analyses based on the symmetry alone are supported by the numerical calculations. The analysis also shows the existence of rotor series for a certain group of states. It also provides interpretations for the relative energies among the four states for the same  $L$  (doublet and quartet, even and odd parities). The symmetry analysis also provides qualitative explanation for the relative energy separation for the first two lowest states within the same symmetry. Section V summarizes the results.

## II. THE ANALYSIS OF THE NODAL STRUCTURES OF WAVE FUNCTIONS

### A. Permutation symmetry of the wave functions

Let the antisymmetrized wave function of the three-electron atom be written as

$$\psi = \sum_s F_s(123) \chi_s^s, \quad (1)$$

where  $i$  ( $i=1,2,3$ ) denotes the spatial coordinates of electron  $i$ , with  $F_s$  being the spatial part and

$$\chi_s^s = \{[\xi(1)\xi(2)]_s \xi(3)\}_s \quad (2)$$

the spin part; the spins of electron 1 ( $e_1$ ) and electron 2 ( $e_2$ ) are coupled to  $s$ ; then  $s$  is coupled to the spin of electron 3 ( $e_3$ ) to form the total spin  $S$ . Let Eq. (1) be rewritten as

$$\begin{aligned} \psi = & \sum_{\mu_1, \mu_2, \mu_3} \delta_{\mu_1 + \mu_2 + \mu_3, M_S} f_{\mu_1 \mu_2 \mu_3}^M(123) \\ & \times \xi_{\mu_1}(1) \xi_{\mu_2}(2) \xi_{\mu_3}(3), \end{aligned} \quad (3)$$

where  $\xi_\mu$  is the spin state with  $\mu = \pm \frac{1}{2}$ ,  $M$  is the  $Z$  component of the total orbital angular momentum  $L$ , and  $M_S$  is the  $Z$  component of  $S$ . Since  $\psi$  is antisymmetrized, we have

$$f_{\mu_1 \mu_2 \mu_3}^M(123) = (-1)^p f_{\mu_{p_1} \mu_{p_2} \mu_{p_3}}^M(p_1 p_2 p_3), \quad (4)$$

where  $p_1 p_2 p_3$  is a permutation of 123 and  $(-1)^p$  is the permutation parity. Owing to Eq. (4), different  $f_{\mu_1 \mu_2 \mu_3}^M$  would provide equivalent information and hence the analysis of only one of them is sufficient to distinguish different states. For our purpose we will analyze  $f_{1/2, 1/2, 1/2}^M(123)$ . This component implies that the spins of electrons 1 and 2 are up, the spin of electron 3 is down, and  $M_S = 1/2$ . Both the doublets  $S = 1/2$  and quartets  $S = 3/2$  are included.

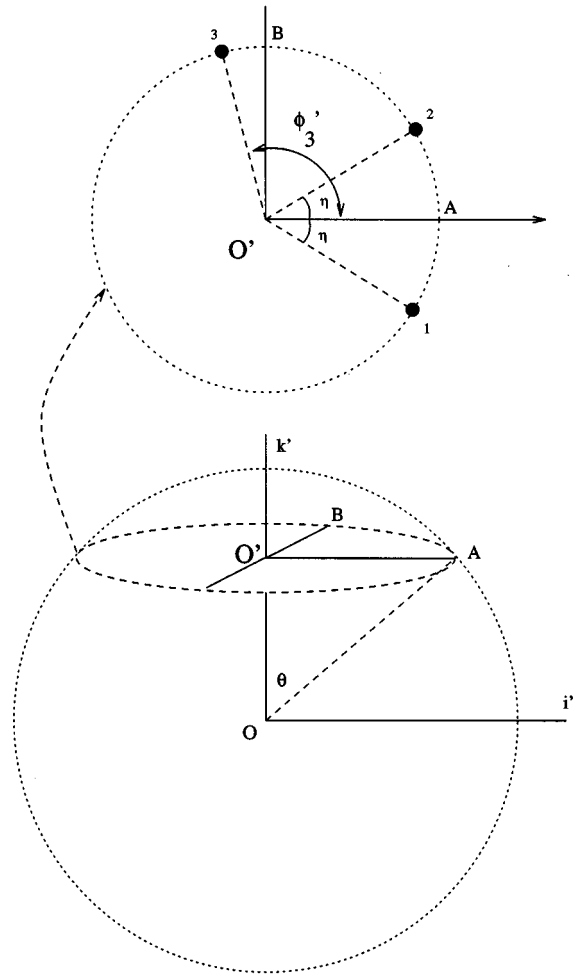


FIG. 1. Body frame of three electrons on a sphere where the center is at point 0. The three electrons labeled (123) form a plane with the  $O'k'$  axis being normal to the plane. The  $O'i'$  axis bisects the two vectors from  $O'$  to electron 1 and from  $O'$  to electron 2. The  $O'j'$  axis lies on the plane and is orthogonal to the  $O'i'$  axis.

### B. Projection of wave functions on the body frame of the electrons

Introduce the body frame  $i'-j'-k'$  with the  $k'$  axis being normal to the plane of the three electrons (refer to Fig. 1); then

$$f_{\frac{1}{2} \frac{1}{2} \frac{1}{2}}^M(123) = \sum_Q D_{QM}^L(-\gamma, -\beta, -\alpha) f_Q(1'2'3'), \quad (5)$$

where  $1'2'3'$  denote the coordinates of the electrons measured in the body frame. The Euler angles  $\alpha, \beta, \gamma$  measure the orientation of the body frame with respect to the fixed laboratory frame. The projection of  $L$  along  $k'$  is  $Q$ , with  $f_Q$  being the  $Q$ -component wave function. Owing to their relation

$$f_{-Q} = \pi(-1)^{L+Q} f_Q^*, \quad (6)$$

where  $\pi$  is the parity, only  $Q \geq 0$  components will be discussed and  $Q$  is taken to be zero or a positive integer for the rest of this paper. From time to time we will refer to  $f_Q$  as the rotational component wave function.

Let  $\vec{r}_i$  be the position of electron  $i$  measured from the nucleus. When  $r_1=r_2=r_3$ , specific constraints are imposed on the wave functions since each wave function has well-defined symmetry properties with respect to rotation, inversion, and permutation of particles. Consequently, specific nodal surfaces may appear in the multidimensional coordinate space. These nodal surfaces originate from the symmetry and they are called the inherent nodal surfaces [15]. Since the wave functions are continuous, these nodal surfaces in turn affect the structure of wave functions in a broad region surrounding the  $r_1=r_2=r_3$  sphere, which in turn affects the relative energy levels of the atom. We set out to examine these constraints in detail and provide some simple interpretation of their origin.

### C. Constraints on the rotational component wave functions by the symmetries at the $r_1=r_2=r_3$ configuration

#### 1. Three electrons forming an isosceles triangle

Referring to Fig. 1, when  $\phi'_3=0^\circ$  or  $180^\circ$ , the three electrons form an isosceles triangle with  $e_1$  and  $e_2$  at the base. In this geometry, a rotation about  $j'$  by  $180^\circ$  together with a space inversion is equivalent to an interchange of  $\vec{r}_1$  and  $\vec{r}_2$ . The former operation causes a change of  $f_Q$  to  $\pi(-1)^{L+Q}f_Q$ , while the latter causes a change of sign since the two electrons  $e_1$  and  $e_2$  have parallel spins. Thus we have the constraint

$$\pi(-1)^{L+Q}f_Q \equiv f_Q^* = -f_Q \quad \text{if } \phi'_3=0^\circ \quad \text{or } 180^\circ. \quad (7)$$

This implies that the real part of  $f_Q$  (denoted by  $f_Q^R$ ) must be zero at  $\phi'_3=0^\circ$  or  $180^\circ$ . In other words, a nodal surface should appear there. The existence of this nodal surface is the result of the inherent symmetry of the wave function and has nothing to do with the interaction potential or the dynamics of the system. Therefore, such nodal surfaces are called inherent nodal surfaces.

For  $Q=0$ , Eq. (7) can be rewritten as

$$\pi(-1)^L f_{0-} = -f_0 \quad \text{if } \phi'_3=0 \quad \text{or } 180^\circ. \quad (8)$$

This implies that  $f_0$  must be zero at  $\phi'_3=0$  or  $180^\circ$  if  $\pi(-1)^L=+1$ .

For  $S=3/2$ , the  $Q=0$  component exhibits more constraints. For  $Q=0$ , the effect of a rotation by  $180^\circ$  about any axis (say the  $j''$  axis) lying on the  $i'-j'$  plane is the same as the rotation by  $180^\circ$  about the  $j'$  axis (the operator of the former rotation is  $e^{i\delta L_3} e^{-i\pi L_2} e^{-i\delta L_3}$ , where  $L_2$  and  $L_3$  are the components of  $L$  along  $j'$  and  $k'$ , respectively;  $\delta$  is the angle from  $j''$  to  $j'$ ; because the eigenvalue of  $L_3$  is zero for  $Q=0$ , the above combination is equal to  $e^{-i\pi L_2}$ ). In addition, for  $S=3/2$ , the interchange of positions of any pair of electrons causes a change of sign. Thus, if  $\phi'_3=3\eta$  (refer to Fig. 1), then  $e_1$  and  $e_3$  will form the base of an isosceles triangle and a rotation about an axis parallel to  $\vec{r}_3-\vec{r}_1$  by  $180^\circ$  together with an inversion is equivalent to an interchange of 1 and 3. Hence, if  $S=3/2$ , Eq. (8) holds also for  $\phi'_3=3\eta$  and similarly for  $\phi'_3=-3\eta$ . Thus Eq. (8) can be generalized to

$$\pi(-1)^L f_0(\mathcal{I}) = -f_0(\mathcal{I}) \quad \text{if } S=3/2, \quad (9)$$

where  $\mathcal{I}$  implies that the electrons form an isosceles triangle irrespective of which two are at the base. Equation (9) implies that  $f_0$  has to be zero for  $\pi(-1)^L=1$  and  $S=3/2$  states at configurations when the three electrons form an isosceles triangle. The fact that nodal surfaces appear at  $\phi'_3=0, 3\eta, 180^\circ$ , and  $-3\eta$  implies that the kinetic-energy term contained in the  $f_0$  component for  $S=3/2$  is particularly large.

#### 2. Coplanar geometry

Another special configuration is the coplanar geometry where the plane of the three electrons also contains the core (or the nucleus) of the atom. In this case, a rotation about  $k'$  by  $180^\circ$  is equivalent to an inversion. Thus we have

$$[1 - \pi(-1)^Q]f_Q = 0 \quad \text{at coplanar structures.} \quad (10)$$

This implies that an inherent nodal surface appears for all the  $Q$  components if  $\pi(-1)^Q=-1$ .

#### 3. Three electrons forming an equilateral triangle

In the cases that the three electrons can form an isosceles triangle, the special geometry of an equilateral triangle further imposes the conditions [16]

$$[1 + 2\cos(2\pi Q/3)]f_Q(\mathcal{E}) = 0 \quad \text{if } S=1/2, \quad (11)$$

$$[1 - \exp(i2\pi Q/3)]f_Q(\mathcal{E}) = 0 \quad \text{if } S=3/2, \quad (12)$$

where  $\mathcal{E}$  denotes the equilateral triangle configuration. The equations above imply that inherent nodal surfaces appear at equilateral configurations in all the  $Q=3m$  ( $m$  an integer) components for  $S=1/2$  states and in all the  $Q \neq 3m$  components for  $S=3/2$  states.

### D. Interpretations in terms of normal modes

We now discuss the implications of the inherent nodal surfaces discussed above.

#### 1. ${}^2S^e$

Consider a  ${}^2S^e$  state as the first example. From Eq. (6),  $f_0^I=0$  (the imaginary part of  $f_0$ ). This is a symmetry forbidden component. For the real part, the constraint (8) implies that an inherent nodal surface occurs at  $\phi'_3=0^\circ$  or  $180^\circ$ .

In Fig. 2(a) the three electrons form an isosceles triangle with  $e_3$  being located at  $C$ , which corresponds to  $\phi'_3=180^\circ$ . With the positions of the two other electrons fixed, the point  $C$  is a local potential minimum on the circle with the smallest Coulomb repulsion between the electrons. A node at  $C$  in general implies that the wave function will have a positive maximum at  $C'$  and a negative minimum at  $C''$ . In other words, if the wave function is positive from  $C'$  to  $C$ , it will be negative from  $C$  to  $C''$ . In Fig. 2(a) this is indicated as a swing motion intuitively where the spin-down electron at the top of the triangle swings left and right around the equilibrium shape. Thus the swing mode is an inherent mode of the  $f_0^R$  component. We summarize this analysis in Table I, using  $s$  to denote that  $f_0^R$  contains an excited swing mode (an excited mode implies that at least a node is contained) and

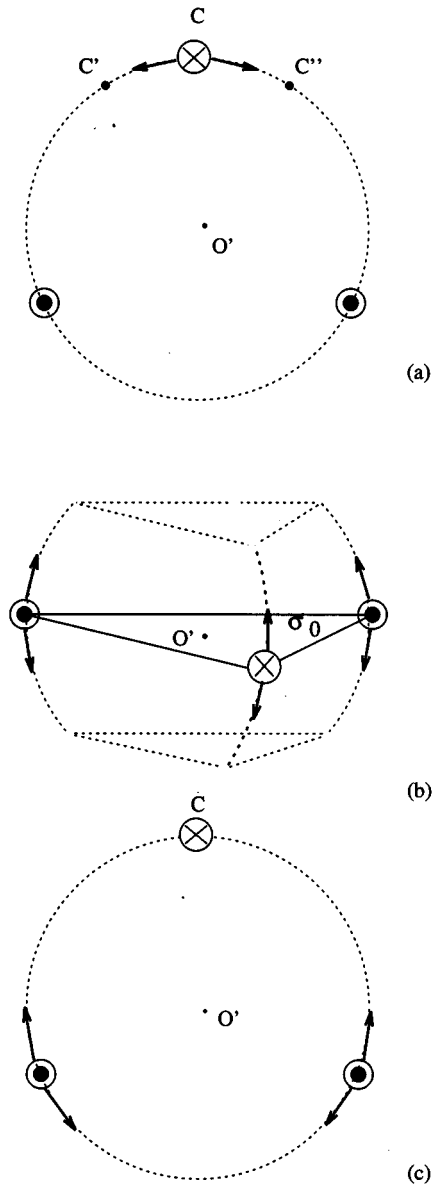


FIG. 2. Intuitive picture of (a) the swing mode ( $s$ ), (b) the  $d$  oscillation mode ( $d$ ), and (c) the hinge mode ( $h$ ) of two spin-up electrons (denoted by a dot in a circle) and one spin-down electron (denoted by a cross in a circle). The plane of the electrons is denoted by  $\sigma_0$  in (b) where the plane moves up and down with respect to the core.

using a black box to indicate that  $f_0^l$  is identically zero or forbidden.

## 2. ${}^4S^o$

Next consider  ${}^4S^o$  states where  $f_0^R$  is forbidden by Eq. (6) and  $f_0^l$  has to follow the constraint (10), which contains a nodal surface at the coplanar configuration. It was found in [17] that such a nodal structure induces a collective oscillation of the electrons, which is called a  $d$ -oscillation mode, where  $d$  is the distance from the nucleus to the plane of the three electrons. In this oscillation the plane of the electrons shifts as a whole from one side of the core to the other repeatedly, as illustrated in Fig. 2(b). Since the coplanar configuration is a local potential minimum and the

$d$ -oscillation mode implies a node at this geometry, this in turn implies that excitation of a  $d$ -oscillation mode will have higher energy. The excitation of a  $d$ -osc mode is labeled by a  $d$  in Table I.

## 3. ${}^2P^e$

For the  ${}^2P^e$  states,  $f_0^R$  is forbidden by Eq. (6),  $f_1^l$  is constrained by Eq. (10), and  $f_1^R$  is constrained by both Eqs. (7) and (10), thus it is labeled by  $d+s$  in Table I for this component. For  $f_0^l$ , this component is constrained by Eq. (11) with the result of having an inherent nodal surface at the equilateral configuration. It was found in [18] that such a nodal surface spoils the stability of an isosceles triangle and induces a hinge mode as depicted intuitively in Fig. 2(c). In this mode, a sharpened isosceles triangle transforms into a flattened one and back repeatedly around the equilateral triangle which is an equilibrium shape. Such a hinge mode is denoted by a label  $h$  for the  $f_0^l$  component in Table I.

## 4. ${}^4S^e$

For  ${}^4S^e$  states,  $f_0^l$  is prohibited by Eq. (6) and  $f_0^R$  is constrained by Eq. (10). This constraint is stronger than Eq. (8), as discussed before, because it has more nodal surfaces. In Table I this stronger swing mode is denoted by  $S$ . Due to the Pauli exclusion principle, the lowest  ${}^4S^e$  intrashell triply excited states can occur only for  $n=4$  shell and higher. They have very high energies compared to other states in the same shell.

So far we have focused on components that are either prohibited or exhibit inherent nodal surfaces. A wave function having such components tends to have higher energies. For states to have lower energies it is preferably to have components that are free from any constraints. These free components are labeled by a blank block in Table I. These components do not have the nodal surfaces of the kind discussed above and the electrons are free to occupy geometrical configurations that can minimize the potential energy. For intrashell states, such a geometry is the coplanar equilateral triangle. However, to achieve the lowest energy, the coplanar equilateral configuration has to be associated with the free components; otherwise the existence of inherent nodal surfaces would increase the internal kinetic energy. For this reason the existence of free components is of particular importance for the low-lying states.

In Table I the existence of forbidden components, free components, as well as the swing mode, the  $d$ -oscillation mode, and the hinge mode and their combinations are tabulated for each rotational component for all the states with  $L \leq 5$ . They are obtained based on the total symmetry of the states and are independent of the dynamics or interaction potentials.

## E. The $r$ -frozen model atom

To provide numerical data for analysis we introduce the  $r$ -frozen model [19], where the three electrons are assumed to be at a fixed distance from the nucleus. In other words, the three electrons are to move only on the surface of a sphere with radius  $r_0$ . In this model, the Hamiltonian is taken to be

TABLE I. Nodal surfaces in the  $f_Q$  components resulting from the inherent symmetry. A black box denotes a forbidden component that is prohibited by symmetry. A blank box denotes a nodeless component that has no nodal surfaces due to the inherent symmetry. The symbol  $s$  implies that there is a nodal surface when the three electrons form an isosceles triangle with the two spin-parallel electrons at the base. The symbol  $S$  is used to indicate that a nodal surface appears whenever the three electrons form an isosceles triangle, irrespective of which two are at the base. The symbol  $d$  implies that there is a nodal surface when the plane of the three electrons coincides with the core (or the nucleus). The symbol  $h$  implies that while the isosceles triangle shape is allowed, an inherent nodal surface appears when the three electrons form an equilateral triangle. The  $s$  and  $S$  denote the swing modes, while  $d$  and  $h$  denote the  $d$  oscillation and the hinge mode, respectively. See Fig. 2 for illustrations.

	$f_0^R$	$f_0^I$	$f_1^R$	$f_1^I$	$f_2^R$	$f_2^I$	$f_3^R$	$f_3^I$	$f_4^R$	$f_4^I$	$f_5^R$	$f_5^I$
$^2S^e$	s											
$^2S^o$		d+h										
$^2P^e$		h	d+s	d								
$^2P^o$	d+s		s									
$^2D^e$	s		d+s	d	s							
$^2D^o$		d+h	s		d+s	d						
$^2F^e$		h	d+s	d	s		d+s	d+h				
$^2F^o$	d+s		s		d+s	d	s	h				
$^2G^e$	s		d+s	d	s		d+s	d+h	s			
$^2G^o$		d+h	s		d+s	d	s	h	d+s	d		
$^2H^e$		h	d+s	d	s		d+s	d+h	s		d+s	d
$^2H^o$	d+s		s		d+s	d	s	h	d+s	d	s	
$^4S^e$	S											
$^4S^o$		d										
$^4P^e$			d+s	d+h								
$^4P^o$	d+S		s	h								
$^4D^e$	S		d+s	d+h	s	h						
$^4D^o$		d	s	h	d+s	d+h						
$^4F^e$			d+s	d+h	s	h	d+s	d				
$^4F^o$	d+S		s	h	d+s	d+h	s					
$^4G^e$	S		d+s	d+h	s	h	d+s	d	s	h		
$^4G^o$		d	s	h	d+s	d+h	s		d+s	d+h		
$^4H^e$			d+s	d+h	s	h	d+s	d	s	h	d+s	d+h
$^4H^o$	d+S		s	h	d+s	d+h	s		d+s	d+h	s	h

$$H = \frac{\hbar^2}{2m_e r_0^2} \sum_i \vec{l}_i^2 + e^2 \sum_{i>j} \frac{1}{|\vec{r}_i - \vec{r}_j|}, \quad (13)$$

where  $\vec{l}_i$  is the orbital angular momentum operator of electron  $i$  with respect to the nucleus  $\vec{r}_i = r_0 \hat{r}_i$ . The value of  $r_0$  is given by 3.3477 Å to simulate the  $n=3$  intrashell states of He<sup>-</sup>. A set of antisymmetrized basis functions constructed out of products of spherical harmonics and spinors coupled to the desired symmetry are then used to diagonalize the Hamiltonian (13) to obtain eigenenergies and eigenfunctions. Even though we concentrate on the  $n=3$  intrashell states, the orbital angular momentum  $l_i$  of each electron ranges from 0 to 4. Thus the calculation is not constrained by the shell model that would require us to consider the range of each  $l_i$  from 0 to 2 only. We remark that the model Hamiltonian (13) employed here is different from the one used in [19], which can be expressed as

$$H_{\text{WL}} = e^2 \sum_{i>j} \frac{1}{|\vec{r}_i - \vec{r}_j|} + \text{const.} \quad (14)$$

This early model did not include the centrifugal potential due to each electron. We will show later that results from the present model are closer to the actual energy separations of intrashell states of atoms.

### III. HIERACHY IN EXCITATION ENERGIES AND THE ORDERING OF LEVELS

In a quantum system, if the Hamiltonian is approximately separable in some coordinates, the excitation energies and the approximate quantum numbers are related to the number of nodes in the coordinates used to describe the system. For easy reference we will assign an index  $i_Q^R$  and  $i_Q^I$  to each of the real and the imaginary parts of the rotational component  $f_Q$  of the wave function. A shorthand notation  $i_Q$  or  $i$  will be used when the specification of the component or of  $Q$  is not essential. Here  $i$  is used to imply that it is related to the number of inherent nodal surfaces of the wave function imposed by the symmetry. Thus  $i=0$  if a rotational component has no node. This component will also be called a nodeless rotational component. We will assign  $i=1$  for having one of the  $s$ -,  $d$ -, or  $h$ -type modes where the rotational wave function has one nodal surface. When one of these modes is excited the state will have higher energy. We will assign  $i=2$  for the  $d+s$  and  $d+h$  types; they have two nodal surfaces. For the  $S$ -type mode, there is more than one nodal surface in the swing mode. We use an index  $i=3$  for these modes. We comment that it may be desirable to further separate the nature of the nodal surfaces as belonging to the  $s$ ,  $d$ ,  $h$ , and other types for a complete description. However, for the global discussion of the three-electron states in this paper such a fine distinction is not essential at this stage.

For a given symmetry, the higher states will acquire additional nodal surfaces since the wave functions of the excited states have to be orthogonal to the wave functions of the lower states. We will assign an index  $v$  to describe such dynamic excitations. If such excitations are not present,  $v=0$  will be assigned. If  $v=1$ , then one new nodal surface is present on top of whatever the number of nodal surfaces

due to the inherent symmetry. In the future it may be desirable to distinguish the additional dynamic nodal surfaces that are associated with the excitation of the  $s$ ,  $d$ , or  $h$  modes.

The  $i$  and  $v$  indices, which are used to designate the number of nodal surfaces due to the inherent symmetry or the dynamical excitation, have been assigned for the real and imaginary parts of each of the rotational component  $f_Q$ . To achieve lower energies a state would prefer to occupy a  $Q$  component that has a smaller total number of nodes. Since it appears that the excitation energies associated with an inherent nodal surface in  $s$ ,  $d$ , or  $h$  as well as a dynamical nodal surface represented by  $v=1$  are comparable, we expect that the excitation energies are measured roughly in the order of increasing total number of nodes, i.e.,  $i+v$ .

In addition to the  $i$  and  $v$  indices, the corresponding  $Q$ , which they are associated with, is also important. In general, when  $L$  is fixed, if the plane of the electrons is perpendicular to  $L$ , it would have a larger moment of inertia and thus a smaller rotational energy. If the plane of the electrons is parallel to  $L$ , then the moment of inertia is smaller and thus a higher rotational energy. Thus a different  $Q$  for a given  $L$  corresponds to a different rotational energy. In general, if  $i$  and  $v$  for the two states are identical, the one with higher  $Q$  will have lower energy. However, we can be sure that  $(i,v)=(1,0)$  and  $(0,1)$  states have higher energies than an  $(i,v)=(0,0)$  state, even if they have different  $Q$ 's since the rotational energy is in general smaller than the excitation of a new nodal surface.

### IV. ANALYSIS OF EXPERIMENTAL AND NUMERICAL RESULTS

We have used the  $r$ -frozen model to calculate many eigenenergies and eigenfunctions of the model Hamiltonian (13). These results will be used in conjunction with available experimental and other theoretical data to support the general conclusion derived from the symmetry consideration alone. In what follows we will use  $^{2S+1}L^\pi(m)$  to denote the states calculated, with  $m=1$  being the lowest state of that symmetry,  $m=2$  the second lowest state, etc., they are called the first state, the second state, etc.

Our next goal is to enumerate the relation between the nodal structure for the  $Q$  components and the relative energies for intrashell states. For comparison, we will use the numerical results from the present  $r$ -frozen model, as well as from the actual calculated energies by Vaeck and Hansen [9] and by Chung and Guo [7], and the results from the analysis of optical spectra documented by Moore [20], if available. In [9] the  $3I3I'3I''$  triply excited states of N<sup>2+</sup> and N<sup>4+</sup> have been calculated. We will not discuss N<sup>4+</sup> since the central field from the nucleus is very strong and the dominant electron-electron interaction addressed here is relatively weakened such that the importance of the nodal constraints may play less of a role from time to time.

Based on the existence of nodal surfaces for different  $Q$  components, we make the following general predictions on the relative energy levels of intrashell states of a three-electron atom.

TABLE II. Maximum magnitudes of the real and the imaginary parts of the rotational component wave functions of the *first* states of the  $3l3l'3l''$  manifold of  $\text{He}^-$ . The components whose wave functions are nodeless are underlined and they are expected to be the dominant components. A blank box indicates that the component is either forbidden (check with Table I) or very small (less than 0.1). The magnitude has been weighted by a factor  $100\sqrt{\alpha/(2L+1)}$ , where  $\alpha=1$  for  $Q=0$  and 2 if  $Q \neq 0$ .

	$f_0^R$	$f_0^I$	$f_1^R$	$f_1^I$	$f_2^R$	$f_2^I$	$f_3^R$	$f_3^I$	$f_4^R$	$f_4^I$
$^2S^e$	3.7									
$^2S^o$		3.9								
$^2P^e$		2.4	0.3	2.8						
$^2P^o$			0.4	<u>3.5</u>						
$^2D^e$	0.5			0.2	1.2	<u>3.5</u>				
$^2D^o$		0.1	1.1	<u>3.7</u>	0.1	0.3				
$^2F^e$		1.0	0.1	0.5	1.0	<u>3.7</u>	0.1	0.1		
$^2F^o$			0.3	<u>3.3</u>	0.1	0.7	1.2	1.0		
$^2G^e$	0.2			0.3	0.6	<u>0.5</u>	0.1	0.1	2.0	<u>3.7</u>
$^2G^o$		0.1	1.2	<u>2.9</u>	0.3	0.8	1.5	1.5	0.9	1.5
$^4S^o$		3.5								
$^4P^e$		<u>3.6</u>								
$^4P^o$			2.4	3.0						
$^4D^e$			0.4	0.5	2.9	2.9				
$^4D^o$		2.8	1.5	1.9						
$^4F^e$		<u>3.0</u>	0.1	0.2	1.4	1.4	0.5	1.1		
$^4F^o$			0.3	0.4			1.6	<u>3.7</u>		
$^4G^o$		0.7	1.0	1.0	0.2	0.2	1.5	<u>3.7</u>		

#### A. The lower states should contain free $Q$ components and these states prefer coplanar equilateral triangular shapes

The free  $f_Q$  component has no inherent nodal surfaces and is allowed to be distributed smoothly around the most favorable coplanar equilateral triangle configuration to lower the potential energy. Thus the low-lying states should contain free  $f_Q$  components, i.e.,  $i_Q=0$  for a certain  $Q$ .

To check this prediction, we examine the relative weights of the  $f_Q$  components for the first states based on the present  $r$ -frozen model calculation and the results are given in Table II. By comparing with Table I, we notice that whenever a free  $f_Q$  is present, that component has the dominant weight. For example, in the  $^2P^o(1)$  state, the maximal magnitude

associated with the free  $f_1^I$  component is one order larger than the  $f_1^R$  component, which is associated with the  $s$  mode, and two orders larger than the  $f_0^R$  component, which is associated with the  $s+d$  mode. The  $f_0^I$  component is identically zero since it is forbidden by the symmetry requirement.

In Table II the weights associated with the  $i_Q=0$  components, i.e., the free components that have  $i=0$ , are underlined and clearly they are the dominant  $Q$  component for each state. The weights shown are for the lowest state (the first state) of each symmetry. Incidentally there are two  $i_Q=0$  components  $Q=2$  and 4 for the  $^2G^e(1)$  state. However, the one with larger  $Q$  is dominant. When  $Q$  is large, the plane of the electrons is more nearly perpendicular to  $L$  and

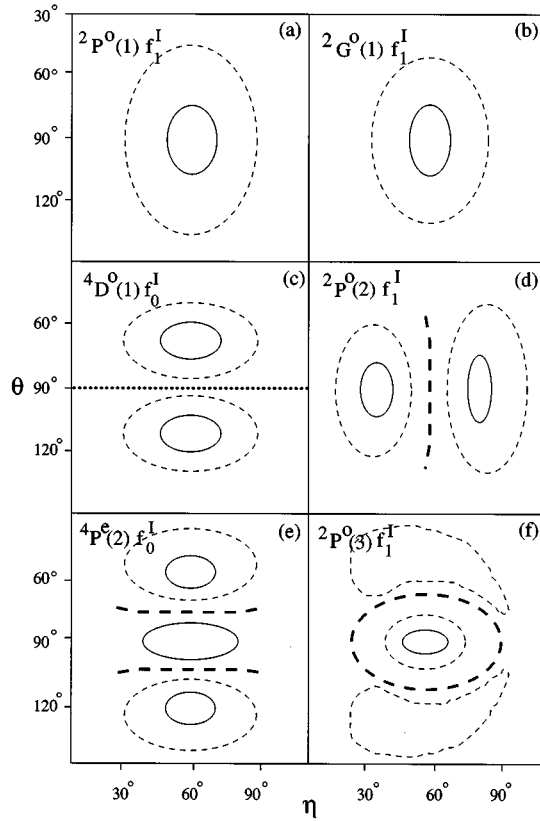


FIG. 3. Selected plots of the real or imaginary part of the rotational component wave functions  $f_Q$  as a function of  $\eta$  and  $\theta$  for  $\phi_3^I=180^\circ$ . Note that at the point  $\eta=60^\circ$  and  $\theta=90^\circ$  the three electrons form a coplanar equilateral triangle. The solid lines indicate contours of 92% of the maximum magnitude and the dashed lines indicate contours of 48% of the maximum magnitude. The thick dotted lines indicate nodal lines that are due to the inherent symmetry of the state. They are due to inherent nodal surfaces. The thick dashed lines indicate nodal lines resulting from the requirement of orthogonality of the excited-state wave functions. They are due to dynamic nodal surfaces. Whenever a nodal line separates the two regions, the signs of the wave function on the two sides are opposites.

thereby the rotational energy is reduced.

We can also explore the wave functions directly from our calculations. Consider the  $i_Q=0$  component of the  ${}^2P^o(1)$  state, i.e., the  $f_1^I$  component. It was found that the optimal value of  $\phi_3^I$  is  $0^\circ$  or  $180^\circ$ . When  $\phi_3^I=180^\circ$ ,  $f_1^I$  as a function of  $\eta$  and  $\theta$  (as specified in Fig. 1) is shown in Fig. 3(a). The wave function peaks at  $\theta=90^\circ$  and  $\eta=62.5^\circ$ , very close to a coplanar equilateral triangle, and it is distributed smoothly around this equilibrium point. Therefore, we can say that the  ${}^2P^o(1)$  state has primarily a coplanar equilateral triangular shape. Figure 3(b) offers another example for  ${}^2G^o(1)$  where

$f_1^I$  has the same shape. In fact, it was found that among all the first states that have one free  $f_Q$  component, the wave functions for that component in the  $\eta$ - $\theta$  diagram all exhibit a peak near the coplanar equilateral triangle geometry. In Table III, the  $\eta$ 's (and  $\theta=90^\circ$ ) where the free  $f_Q$  component peaks for each first state are shown. They are all very close to  $60^\circ$ , indicating the preferential geometry of a coplanar equilateral triangle.

Table III also shows that the most probable shape for  $S=3/2$  states is an exact coplanar equilateral triangle. For  $S=1/2$  states, the most probable geometry is a flattened or a sharpened isosceles triangle. A possible explanation is that the electron-electron correlation between a spin-parallel pair and a spin-antiparallel pair are not equal in  $S=1/2$  states. Another point worth mentioning is that for  $S=1/2$ , if the free  $f_Q$  component is for  $Q=L$ , then the deviation from the equilateral triangle is small. Otherwise, the deviation is larger. A possible explanation is that the centrifugal force does not alter the equilateral geometry for  $Q=L$  components, but does distort the geometry for the  $Q \neq L$  components. In general, if the free component is associated with a large  $L$  and a small  $Q$ , it will have a higher rotational energy and thus has to compete with other  $f_Q$  components. These states correspond to cases where the mixing of different  $Q$  components is significant and thus  $f_Q$  is not very ‘‘pure.’’

### B. Relative energies of the ${}^2L^e(1)$ , ${}^2L^o(1)$ , ${}^4L^e(1)$ , and ${}^4L^o(1)$ states and the inherent nodal surfaces

Among the four states with the same  $L$ , if the coplanar equilateral triangle geometry is accessible, this state will have the lowest energy. If there exists more than one such state, then the one with larger  $Q$  will have the lower energy. If the coplanar equilateral triangle shape is not allowed, then the state with fewer inherent nodal surfaces will have less energy.

From this general rule, the relative energies of the  $L$  quartet can be more or less predicted. We will refer all the calculated energies with respect to the  ${}^2P^o(1)$  state, which has the lowest energy. In the following discussion the reader is reminded to consult Table I often.

#### 1. $L=0$

Consider the  $L=0$  quartet. None of them has free  $f_Q$  components and in general they have higher energies. Among the four, the  ${}^2S^e$  has an  $s$  mode, the  ${}^4S^o$  has a  $d$  mode, both contain one internal nodal surface, and their energies should be close to each other. The  ${}^2S^o$  has a  $d+h$  mode and its energy is higher because of more internal nodal surfaces. The  ${}^4S^e$  has the highest energy since it has an  $S$  mode, which has the most nodal surfaces.

TABLE III. Most probable shape possessed by the first states that have nodeless rotational component wave functions. The table gives  $\eta$  (refer to Fig. 1), where the wave function is maximum for  $\phi_3^I=180^\circ$  and  $\theta=90^\circ$ . When  $\eta=60^\circ$ , it is a coplanar equilateral triangle. For  ${}^2G^e(1)$  the  $Q=4$  component is used.

${}^2P^o$	${}^2D^e$	${}^2D^o$	${}^2F^e$	${}^2F^o$	${}^2G^e$	${}^2G^o$	${}^4P^e$	${}^4F^e$	${}^4F^o$	${}^4G^o$
62.5°	60.5°	54.3°	58.3°	69.4°	60.7°	47.8°	60.0°	60.0°	60.0°	60.0°

TABLE IV. Ordering of levels of the first states  $^{2S+1}L^\pi(1)$  of three-valence-electron atoms (ions) from experimental spectra. For a given species and  $L$ , the energy increases in going down along the column. Data are from [20].

	B			C <sup>+</sup>			N <sup>2+</sup>					
$n=2$	$^2S^e$	$^2P^o$	$^2D^e$	$^2S^e$	$^2P^o$	$^2D^e$	$^2S^e$	$^2P^o$	$^2D^e$			
		$^4P^e$		$^4S^o$	$^4P^e$	$^2D^o$	$^4S^o$	$^4P^e$	$^2D^o$			
					$^2P^e$			$^2P^e$				
	Al			Si <sup>+</sup>			P <sup>2+</sup>			S <sup>3+</sup>		
$n=3$	$^2S^e$	$^2P^o$	$^2D^e$	$^2F^o$	$^2S^e$	$^2P^o$	$^2D^e$	$^2F^o$	$^2S^e$	$^2P^o$	$^2D^e$	
		$^4P^e$			$^4S^o$	$^4P^e$			$^4S^o$	$^4P^e$	$^4D^o$	
						$^2P^e$				$^2P^e$		
						$^4P^o$				$^4P^o$		
	Ga			Ge <sup>+</sup>			As <sup>2+</sup>					
$n=4$	$^2S^e$	$^2P^o$	$^2D^e$	$^2F^o$	$^2S^e$	$^2P^o$	$^2D^e$	$^2F^o$	$^2G^e$	$^2S^e$	$^2P^o$	$^2D^e$
		$^4P^e$				$^4P^e$					$^4D^o$	
						$^2P^e$					$^2P^e$	
						$^4P^o$					$^4P^o$	
	In			Sn <sup>+</sup>			Sb <sup>2+</sup>					
$n=5$	$^2S^e$	$^2P^o$	$^2D^e$	$^2F^o$	$^2S^e$	$^2P^o$	$^2D^e$	$^2F^o$	$^2G^e$	$^2S^e$	$^2P^o$	$^2D^e$
		$^4P^e$				$^4P^e$					$^4D^o$	
						$^2P^e$					$^2P^e$	
						$^4P^o$					$^4P^o$	
	Tl			Pb <sup>+</sup>			Bi <sup>2+</sup>					
$n=6$	$^2S^e$	$^2P^o$	$^2D^e$	$^2F^o$	$^2S^e$	$^2P^o$	$^2D^e$	$^2F^o$	$^2G^e$	$^2S^e$	$^2P^o$	$^2D^e$
		$^4P^e$				$^4P^e$					$^4D^o$	
						$^2P^e$					$^2P^e$	

Let us check the actual energies calculated for these four states. For He<sup>-</sup>, the calculated energies for the three  $n=3$  intrashell states  $^4S^o$ ,  $^2S^e$  and  $^2S^o$  from the present model are 1.71, 1.75, and 4.83 eV, respectively. (The  $^4S^e$  state does not exist for the  $n=3$  states.) In [9], for N<sup>2+</sup>, the calculated energies are 5.82, 4.68, and 11.03 eV, respectively. When our  $r$ -frozen model is generalized to the  $n=4$  intrashell triply excited states for He<sup>-</sup> using  $r_0=5.95$  Å as suggested in [19], we obtained 0.658 and 0.699 eV for  $^4S^o$  and  $^2S^e$ , 1.749 eV for  $^2S^o$ , and 3.018 eV for  $^4S^e$ , respectively. Thus the prediction above is well confirmed.

Let us also check the realistic atomic energy levels from experimental data [20]. The known intrashell energy level data from the 16 three-valence-electron atomic and ionic species ranging from  $n=2$  to  $n=6$  shells have been collected in Table IV. For  $L=0$ , if the two  $^2S^e$  and  $^4S^o$  states are known, they are in the order predicted.

## 2. $L=1$

Next consider the four  $L=1$  states. The two states  $^2P^o$  and  $^4P^e$  can access a coplanar equilateral triangular shape and their energies are lower. Between the two, the free component is  $Q=1$  for  $^2P^o$  and  $Q=0$  for  $^4P^e$ , thus the  $^2P^o$  state is lower. The other two states will have higher energies since they contain nodal surfaces in all the  $f_Q$  components, but their relative values cannot be obtained simply from the symmetry rule.

From the actual calculation using the  $r$ -frozen model for the  $n=3$  intrashell triply excited states of He<sup>-</sup>, the energies

for  $^2P^o$ ,  $^4P^e$ ,  $^2P^e$ , and  $^4P^o$  are 0, 0.23, 1.71, and 2.34 eV, respectively. For N<sup>2+</sup> the corresponding energies are 0, 1.38, 4.94, and 5.32 eV. For the  $n=2$  intrashell triply excited states of Li, the accurate energies [7] for the three states  $^2P^o$ ,  $^4P^e$ , and  $^2P^e$  are 0, 0.296, and 4.666 eV, respectively. The predicted energy ordering is nicely reflected in the calculations. Inspection of the experimental results shown in Table IV shows clearly that the prediction is also confirmed.

## 3. $L=2$

For the  $D$  quartet, the two states  $^2D^e$  and  $^2D^o$  have free  $f_Q$  components  $Q=2$  and  $Q=1$ , respectively, thus the  $^2D^e$  state is the lowest. The other two states both possess components with inherent nodal surfaces and thus the energies are higher. The energies for the four states  $^2D^e$ ,  $^2D^o$ ,  $^4D^o$ , and  $^4D^e$  are 0.65, 1.19, 2.37, and 3.00 eV, respectively, from our model calculations for He<sup>-</sup>. For N<sup>2+</sup>, the corresponding energies [9] are 2.02, 3.73, 5.20, and 8.48 eV, respectively. For the  $n=2$  intrashell triply excited states of Li, the calculated energies [7] for  $^2D^e$  and  $^2D^o$  states are 2.506 and 4.660 eV. All of these calculations confirm the predicted ordering. Furthermore, the experimental data in Table IV confirm that the  $^2D^e$  is the lowest state and  $^2D^o$  is the second lowest state. For S<sup>3+</sup>, the  $^4D^o$  state has been observed, but not the  $^2D^o$  state. According to the rule above, the  $^2D^o$  state should lie between  $^2D^e$  and  $^4D^o$  states.

## 4. $L=3$

All of the four states have free  $f_Q$  components, with  $Q=3,2,1,0$  for  $^4F^o$ ,  $^2F^e$ ,  $^2F^o$ , and  $^4F^e$ , respectively. This

order in turn applies to the energies of these four states. Compared to the calculated values for  $\text{He}^-$ , the  $r$ -frozen model gives 1.56, 2.35, 2.49, and 2.61 eV, respectively, while for  $\text{N}^{2+}$  they are 4.02, 6.54, 6.43, and 7.69 eV. The latter has a change of the relative order between  ${}^2F^e$  and  ${}^2F^o$ , but the energy difference between the two states is small. Note that the energy differences among these four states are understood to be due to the relative orientation of the coplanar equilateral triangle with respect to the direction of  $\vec{L}$ . In Table IV we have listed the  ${}^2F^o$  state to be the head state of the four. All the other three  $L=3$  states have not been observed; thus a test of the present rule is not possible.

### 5. $L=4$

Three of the four states have free  $f_Q$  components,  $Q=4$  and 2 for  ${}^2G^e$ ,  $Q=3$  for  ${}^4G^o$ , and  $Q=1$  for  ${}^2G^o$ . Thus the expected energy ordering should be  ${}^2G^e$ ,  ${}^4G^o$ ,  ${}^2G^o$ , and  ${}^4G^e$ . For the  $n=3$  intrashell states, the last one is not allowed. This prediction is to be compared with the calculated values 2.64, 3.66, and 4.15 eV for  $\text{He}^-$  and 7.99, 9.52, and 11.27 eV for  $\text{N}^{2+}$ . When the  $r$ -frozen model is used for the  $n=4$  intrashell states, the calculated energies for the four states are 0.83, 1.14, 1.35, and 1.56 eV, confirming the prediction. In Table IV the only experimental data is for the  ${}^2G^e$  state, which is assigned to be the lowest state.

### 6. $L=5$

All the four states have free  $f_Q$  components  $Q=5$  and 1 for  ${}^2H^o$ ,  $Q=4$  and 2 for  ${}^2H^e$ ,  $Q=3$  for  ${}^4H^o$ , and  $Q=0$  for  ${}^4H^e$ . When there are two  $Q$  components accessible, the larger  $Q$  will be the dominant one. Thus the predicted energies in increasing order will be  ${}^2H^o$ ,  ${}^2H^e$ ,  ${}^4H^o$ , and  ${}^4H^e$ . For the  $n=3$  intrashell states the two quartet states are not allowed. The  ${}^2H^o$  and  ${}^2H^e$  state energies calculated for  $\text{He}^-$  and  $\text{N}^{2+}$  are 3.99 and 5.31 eV and 11.94 and 14.49 eV, respectively. For the  $n=4$  intrashell states of  $\text{He}^-$ , the  $r$ -frozen model gives 1.26, 1.67, 1.82, and 2.03 eV, respectively, in the order as predicted. We have found only one  $L=5$  state in the experimental data in  $\text{Bi}^{2+}$ , and this state is the lowest  ${}^2H^o$  state.

### C. The Rotor series

The existence of truncated rotor series is well understood for doubly excited states of atoms. The states within the series are known to have similar internal structure. All the intrashell states discussed above that have nodeless rotational components are shown to have coplanar equilateral triangle shapes and they have nearly conserved  $Q$ . By grouping these states that have identical dominant  $Q$ , we explore if these states form a rotor series as in the case for doubly excited states. If there is more than one nodeless rotational component, the first state will have the larger  $Q$  and the second state will have the smaller  $Q$ . The rotor series can be grouped according to the total spin, the dominant  $Q$ , and the parity  $\pi$  and each series is denoted by  $(SQ\pi)$ . Referring to Table I, it is clear that we can observe the following series:

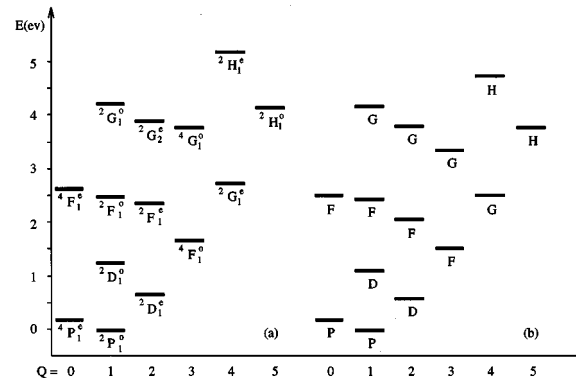


FIG. 4. Selective calculated energy levels of the  $3/3l'3l''$  states of  $\text{He}^-$  rearranged in rotor series. Each of these states has a rotational component whose imaginary part  $f_Q^i$  has no nodes. The rotor series is obtained by grouping these states that have the same  $Q$ . (a) shows the rotor series using energies obtained from the actual model calculations. (b) shows the rotor series expected out of a rigid rotor. In (a) the subscript  $i$  is used to denote the  $i$ th lowest state of that symmetry.

$(3/2\ 0\ e)$  containing  ${}^4P^e(1)$ ,  ${}^4F^e(1)$ ,  ${}^4H^e(1)$ , ...

$(1/2\ 1\ o)$  containing  ${}^2P^o(1)$ ,  ${}^2D^o(1)$ ,  ${}^2F^o(1)$ ,  
 ${}^2G^o(1)$ , ...

$(1/2\ 2\ e)$  containing  ${}^2D^e(1)$ ,  ${}^2F^e(1)$ ,  ${}^2G^e(2)$ , ...

$(3/2\ 3\ o)$  containing  ${}^4F^o(1)$ ,  ${}^4G^o(1)$ ,  ${}^4H^o(1)$ , ...

$(1/2\ 4\ e)$  containing  ${}^2G^e(1)$ ,  ${}^2H^e(1)$ , ...

$(1/2\ 5\ o)$  containing  ${}^2H^o(1)$ , ...

The existence of these rotor series was suggested in [19], but the model Hamiltonian used there is more limited and the pattern is not very clear, as discussed in Sec. II E.

To check the validity of the rotor series model, we compare the calculated energy levels from the present model with the energies expected from a rigid rotor given by

$$E_{\text{rot}} = \frac{\hbar^2}{2} \left( \frac{L_1^2}{I_1} + \frac{L_2^2}{I_2} + \frac{L_3^2}{I_3} \right), \quad (15)$$

where  $I_i$  is the moment of inertia with respect to the  $i$ th body axis. If the three electrons form a rigid coplanar equilateral triangle with the third axis normal to the plane, then  $I_1 = I_2 = I_3/2$ . In this case the rotational energy can be written as

$$E_{\text{rot}} = \frac{\hbar^2}{2I_3} [2L(L+1) - Q^2], \quad (16)$$

where  $I_3 = 3m_e r_0^2$ . Inserting the  $r_0$  used in the present calculation, the energy spectrum of the rigid rotor is compared with the calculated energies in Fig. 4. The strong similarity between Figs. 4(a) and 4(b) implies that the energy difference in this group arises essentially from the collective rotation. In Fig. 4 each of the  $(S, Q, \pi)$  rotor series discussed above (except the one represented by  $Q=5$ ) is represented. The rotational energy depends strongly on  $Q$ ; the larger the

$Q$ , the smaller the rotational energy  $E_{\text{rot}}$  that is characteristic of an oblate rotor. This feature is clear in the present model, as shown in Fig. 4(a); but not in [19] since the latter model neglects the first term in the Hamiltonian (13). Accordingly, the  $Q$  dependence of the rotational energy in [19] has errors. Furthermore, the  $Q$  designations for some states there were wrong. Specifically, the dominant  $Q$  for  ${}^2G^e(1)$  is 4 (not 2), for  ${}^2G^e(2)$  it is 2 (not 4), for  ${}^2H^o(1)$  it is 5 (not 1), and for  ${}^2H^e(1)$  it is 4 (not 2). Once the  $Q$  designations have been corrected, the energy levels calculated by Vaeck and Hansen [9] (the  $A'$  group in Fig. 3 of their paper) for  $\text{N}^{2+}$  do indeed show rotor series similar to Figs. 4(a) and 4(b). The spectrum of the corresponding states of  $\text{N}^{4+}$  in [9] is also qualitatively similar, but there are a few deviations from the order of the rigid rotor. The fact that energy spectrum for the  $3l3l'3l''$  states for  $\text{He}^-$  from the model calculation and for  $\text{N}^{2+}$  from the configuration-interaction calculation both display the rotor structure is very appealing and renders the analysis of wave functions in the body frame of the three electrons a very attractive approach.

Let us explore the rotor structure in more detail. Note that the lowest member of each of the rotor series, except for the first series that starts with  ${}^4P^e$ , all have  $Q=L$ . Accordingly,  $E_{\text{rot}} = \hbar^2 L(L+2)/2I_3$ . If the rigid rotor description is correct and if the energy is measured from the lowest state  ${}^2P^o$ , then the expected ratios for  $E({}^2D^e)/E({}^4F^o)$ ,  $E({}^2G^e)/E({}^4F^o)$ , and  $E({}^2H^o)/E({}^4F^o)$  are 0.417, 1.75, and 2.667, respectively. The same ratios from our model calculations are 0.417, 1.70, and 2.56, while for  $\text{N}^{2+}$  from [9] the ratios are 0.50, 1.74, and 2.97. There are deviations from a rigid rotor, but the deviations are not large.

We have predicted that for  $nl n l' n l''$  states, the  ${}^2P^o$  and  ${}^4P^e$  are the two lower states for  $L=1$  and  ${}^2D^e$  and  ${}^2D^o$  are the two lower states for  $L=2$ . All of them have nodeless rotational components and their energies are differentiated mostly by the rotational excitation. On the other hand, all the  $L=0$  states do not have nodeless rotational components; thus their energies are higher. We can check how well the actual atomic energy levels follow this ordering. For  $\text{He}^-$  the excitation energies for  ${}^2P^o$ ,  ${}^4P^e$ , and  ${}^2D^e$  ( $n=2$ ) are known at 57.22, 57.42, and 58.28 eV, respectively. This is also the correct order for  $\text{C}^+$ . The order of these three states also exists in many other atoms and ions with three valence electrons. Using the independent-particle model, these three states have the electronic configurations of  $ns^2np$ ,  $nsnp^2$ , and  $nsnp^2$ , respectively. However, it is well known that the  $3s3p^2$   ${}^2D^e$  and  $3s^23d$   ${}^2D^e$  interact strongly from the configuration mixing viewpoint [21]. The energy ordering of these states is easily understood as rotational excitations of a rotor instead.

#### D. First states where the rotational components have inherent nodal surfaces

The states discussed in Sec. IV C belong to those where at least one rotational component of the wave function has no nodes. From Table I it is clear that there are states where all the rotational components exhibit one form of nodal surface or another. They are distinguished by  $s$ ,  $d$ ,  $h$ , and  $S$  as explained earlier. As an example, consider  ${}^4D^o$ . From Table I we note that  $f_0^R$  is forbidden,  $f_0^I$  is a  $d$ ,  $f_1^R$  is an  $s$ ,  $f_1^I$  is an

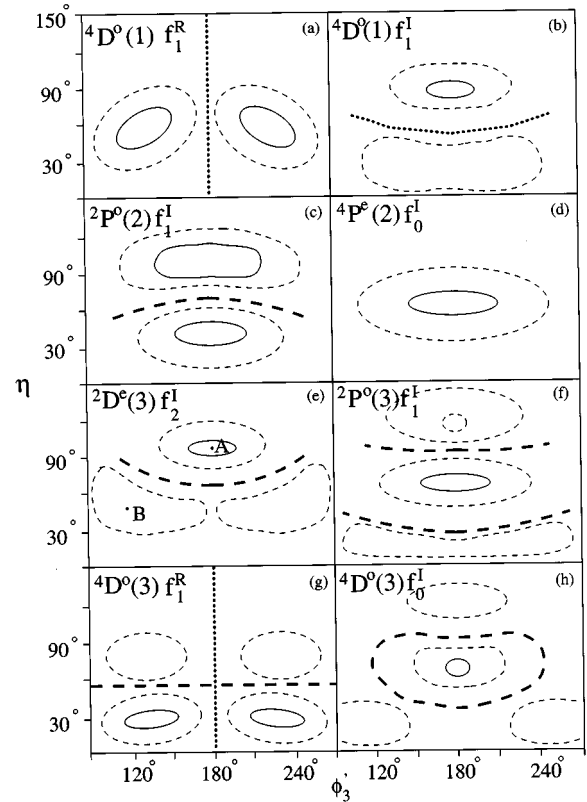


FIG. 5. Selected plots of the real or imaginary part of the rotational component wave functions  $f_Q$  as a function of  $\phi_3'$  and  $\eta$ . The  $\theta$  is given at  $90^\circ$  in (a)–(g), but is given at  $75^\circ$  in (h). All the symbols are the same as in Fig. 3.

$h$ ,  $f_2^R$  is a  $d+s$ , and  $f_2^I$  is a  $d+h$ . The last two components  $f_2^R$  and  $f_2^I$  have small amplitudes (see Table II) because each has two nodal surfaces. For the other three components  $f_0^I$ ,  $f_1^R$ , and  $f_1^I$  their relative magnitudes are about equal. We thus conclude first that there is no dominant  $Q$  component, i.e., the mixing among the rotational components is large and we thus should not expect rotor series to exist here.

We next examine the nature of each rotational component using the wave function generated from the  $r$ -frozen model. The  $d$  mode of the  ${}^4D^o$  state (the  $f_0^I$  component) was found to have the maximum of the wave functions when  $\phi_3' = 180^\circ$ . When we fix  $\phi_3' = 180^\circ$ , the rotational component of the wave function can be plotted in the  $\eta$ - $\theta$  plane, as shown in Fig. 3(c), where the maximum and the minimum of the wave function occur at  $\theta = 90^\circ \pm 23^\circ$ , respectively, with a nodal line at  $\theta = 90^\circ$  (indicated by a thick dotted line). Such a wave function illustrates an excited  $d$ -oscillation mode. The  $f_1^R$  and  $f_1^I$  components display  $s$  and  $h$  modes, respectively. They have the maximum at  $\theta = 90^\circ$ , i.e., they have coplanar structure. By fixing  $\theta = 90^\circ$ , the wave functions on the  $\phi_3'$ - $\eta$  plane are shown in Figs. 5(a) and 5(b), respectively. In Fig. 5(a) there is a maximum at  $\phi_3' = 180^\circ + 44^\circ$  and a minimum at  $180^\circ - 44^\circ$ . From the definition of  $\phi_3'$ , this is clearly a swing of electron 3 with respect to electrons 1 and 2. The swing is coplanar with a nodal line at  $\phi_3' = 180^\circ$  (indicated by a thick dotted line). In Fig. 5(b) there is no nodal line along  $\phi_3'$ , but there is a nodal line (indicated by a thick dotted line) along  $\eta$ , with the maximum at  $\eta = 89^\circ$

(flattened isosceles triangle) and a minimum at  $\eta=39^\circ$  (sharpened isosceles triangle). This implies a coplanar hinge motion with a nodal line at  $\eta=60^\circ$  (the coplanar equilateral triangle).

It turns out that the above analysis is quite general for all the  $d$ ,  $s$ , and  $h$  modes. Figures 3(c), 5(a), and 5(b) are typical of the  $d$ ,  $s$ , and  $h$  components, respectively, where the inherent nodal lines are model independent. Thus the basic modes are embedded in the rotational component of the wave function via the existence of nodal surfaces. The existence of these nodal surfaces implies higher excitation energies. On the other hand, each state has several different modes coexisting among the different rotational components; thus there is not a single dominant  $f_Q$  component. Such states are said to have strong mode mixing or  $Q$  mixing. In general, it is more difficult to predict the relative energies of mode-mixing states. They do not have the rotor structure since the latter requires an approximate conserved  $Q$ .

### E. Second states where the rotational components are excited

So far we have discussed the wave functions of states where the rotational components are not dynamically excited, including those components that exhibit inherent nodal surfaces. For states at higher energies, some of the rotational components can be dynamically excited as well (e.g.,  $v \neq 0$ ). Clearly, the next group of higher-energy states are those where the nodeless rotational components are excited. This subsection examines the nature of these excitations.

In Figs. 3(d) and 5(c) we consider the second state of the  ${}^2P^o$  symmetry, i.e., the  ${}^2P^o(2)$  state. Comparing Fig. 3(d) with Fig. 3(a), we note that the  ${}^2P^o(2)$  state has an additional nodal line at  $\eta=60^\circ$  (indicated by a thick dashed line). For this state, there is no node in  $\phi'_3$ . Thus the second state acquires a new hinge mode ( $h$ ) and no  $d$ -oscillation ( $d$ ) or swing ( $s$ ) modes are produced. This has been found to be the case for the  $S=1/2$  states.

In Figs. 3(e) and 5(d) we consider the  ${}^4P^e(2)$  state. For  ${}^4P^e(1)$  the component  $f'_0$  is nodeless, but from Fig. 3(e) we note that this component for the second state has a pair of nodal lines in  $\theta$  symmetric with respect to  $\theta=90^\circ$ . This means that it is an excitation of the  $d$ -oscillation mode (indicated by two thick dashed lines). Together with Fig. 5(d), this shows that for the  ${}^4P^e(2)$  state, the  $d$ -oscillation mode is excited but the swing and the hinge modes are not excited. This has been found to be true for the second states for  $S=3/2$ . The fact that  $s$  and  $h$  modes are not excited means that  $S=3/2$  states can keep the shape of an equilateral triangle better than the  $S=1/2$  states.

For states with even higher energies, say, the third state of a given symmetry, the coupling between the modes may appear. Consider the nodeless rotational component  $f'_2$  for the  ${}^2D^e(3)$  state, as shown in Fig. 5(e). The evolution from  $A$  to  $B$  (see the figure) implies a decrease in  $\phi'_3$  as well as a decrease in  $\eta$ , thus the swing and the hinge modes are coupled. The coupling of different modes is quite common for higher excited states. Another example is shown in Figs. 3(f) and 5(f) for the  $f'_1$  component of the  ${}^2P^o(3)$  state. Together they show the coupling of the  $d$ -oscillation and the hinge modes.

We emphasize that the additional nodal lines (or surfaces) discussed in this subsection for the nodeless rotational components are not due to the inherent symmetries of the states. They are the results of the higher quanta of the elementary normal modes and they are called the dynamic nodal surfaces. In Figs. 3 and 5 we have used thick dotted lines to denote inherent nodal surfaces and thick dashed lines to denote dynamic nodal surfaces.

For rotational components that have intrinsic nodal surfaces, excitation in that component in general is accompanied by the excitation of other modes. For example, the  $f'_1$  component for the  ${}^4D^o$  symmetry is a swing mode, but its third state acquires an additional hinge mode, as can be seen in Fig. 5(g). An example of the excitation of the  $d$  component is given in Fig. 5(h), where the  $\eta$ - $\phi'_3$  plot is given for  $\theta=75^\circ$ . An identical pattern but of opposite sign in wave function appears at  $\theta=105^\circ$ . In this case, the  $d$ -oscillation mode is accompanied by the occurrence of the coupling of the swing and the hinge modes. Other examples can be found in Fig. 3(b) of [10] for the  ${}^2S^e(2)$  state and Fig. 2b of [11] for the  ${}^4S^o(2)$  state.

The excited states of a given symmetry do not necessarily correspond to the excitation of a  $Q$  component. With respect to the nodeless rotational component of the lowest state of a symmetry, the second state of the same symmetry can achieve orthogonality by having a new dynamic nodal surface in the same  $Q$  component or by acquiring amplitudes in other  $Q$  components that have intrinsic nodal surfaces of the  $s$ ,  $d$ , or  $h$  types or their combinations. In either case, the existence of nodal surfaces implies higher excitation energies, but there is no *a priori* rule of knowing which one will have lower energies. In most cases the excitation energies are comparable, thus resulting in strong mixing of the  $Q$  components. Such strong mixings are shown in Table V, where the relative magnitude of the rotational components for the second states are given. Again, the entries that are underlined belong to the free components. Unlike the case for the first state, in Table V these components are no longer dominant, thus implying strong  $Q$  mixing. We further comment that for the second state of a given symmetry, it was found that those  $Q$  components that have intrinsic nodal surfaces do not have additional dynamic nodal surfaces. In fact, the  $Q$  components that are excited with comparable weights have essentially identical numbers of nodal surfaces, i.e.,  $i+v$  is identical.

### F. Relative energy separations between the first and second states

In analyzing the first states we have shown that it is important to enumerate the nodal structure of each of the rotational component  $f_Q$ . For the first states there are no dynamical nodal surfaces. The dominant  $Q$  component for the first state is the one that has the fewest inherent nodal surfaces. We can thus characterize each first state by the indices  $i, v=0, Q$  for the specific  $Q$  component. For the second state of each symmetry, the state will try to lower its energy, but under the constraint that its wave function be orthogonal to the first state. This implies that the way the second state is excited depends much on the inherent nodal structure of the rotational components of each symmetry, which in turn de-

TABLE V. Same as Table II, but for the second state of each symmetry.

	$f_0^R$	$f_0^I$	$f_1^R$	$f_1^I$	$f_2^R$	$f_2^I$	$f_3^R$	$f_3^I$	$f_4^R$	$f_4^I$
${}^2S^e$	4.2									
${}^2S^o$		3.9								
${}^2P^e$		3.3	0.7	2.2						
${}^2P^o$			2.8	<u>2.6</u>						
${}^2D^e$			0.3	2.5	1.3	<u>1.8</u>				
${}^2D^o$		0.1	1.4	<u>1.8</u>	1.0	3.1				
${}^2F^e$		1.0	1.0	2.8	1.3	<u>1.7</u>	0.2	0.3		
${}^2F^o$	0.5		0.4	<u>1.0</u>	1.0	2.2	1.5	2.5		
${}^2G^e$	1.0		0.1	0.5	1.1	<u>2.7</u>	0.2	0.5	1.6	<u>1.6</u>
${}^2G^o$		0.3	0.9	<u>1.8</u>	0.5	0.6	0.6	0.9	1.6	3.0
${}^4S^o$		3.7								
${}^4P^e$		<u>3.3</u>	1.3	1.6						
${}^4P^o$			3.2	3.3						
${}^4D^e$			1.4	1.7	2.0	2.5				
${}^4D^o$		1.8	2.9	3.1	0.4	0.4				
${}^4F^e$		<u>1.8</u>	0.3	0.4	0.7	0.7	1.4	3.1		
${}^4F^o$			1.9	2.7	1.4	1.4	0.7	<u>1.8</u>		
${}^4G^o$		2.4	0.9	1.0	1.2	1.2	1.1	<u>1.8</u>	0.5	0.6

termines the energy separation between the first two states. By analyzing the nature of nodal surfaces for the rotational components as given in Table I, we can draw the following general conclusions on how the second state is excited for each symmetry.

### 1. Dynamic excitation of the same rotational component

Table I shows that the  ${}^4P^e$  state contains a free component ( $Q=0$ ) and an  $i=2$  component ( $Q=1$ ). The free component is already occupied by the first state and thus  $(i,v,Q)=(0,0,0)$  for this state. For the second state, there are two choices: either to occupy the free component again but with one additional dynamic nodal surface  $(i,v,Q)=(0,1,0)$  or to occupy the  $i=2$  component  $(i,v,Q)=(2,0,1)$ . Since the total number of nodal surfaces  $i+v$  is smaller for the former, it is the preferred choice for the second state. This choice was indeed confirmed as seen

in Table V, where the weight for the second state is dominated by the  $Q=0$  component, indicating that the second state is mostly due to the excitation of the free component. Since the coplanar equilateral triangle configuration in the free component is very stable, it is rather difficult to excite. Thus the energy separation between the first and the second states for the  $v=1$  type excitation in general is rather large. From Table I, the second state for the  ${}^2P^o$  symmetry clearly belongs to this type as well.

### 2. Excitation of a different $Q$ component where $i_Q=1$

Consider the  ${}^2D^o$  states where, besides the free component, two  $i=1$  components are contained. Since the first state has  $(i,v,Q)=(0,0,1)$ , the second state can achieve orthogonality by occupying the  $Q=2$  component ( $i=1$ ) without exciting the  $Q=1$  component, i.e., having  $(i,v,Q)=(1,0,2)$ . In Table V we see that the most important component in the  ${}^2D^o(2)$  state is indeed the excitation of the  $d$  mode with  $Q=2$  rather than the free component with  $Q=1$ . Analysis of the wave function shows that in the second state all of its rotational components have  $i+v=1$ ; i.e., an additional dynamic nodal surface is present for the  $Q=1$  component. Although the free component is excited, its weight is small. We thus expect that the energy separation between the first and the second states will be smaller for this type than for the type discussed in Sec. IV F 1. From Table I we can identify that the second state for  ${}^2D^e$  also belongs to this type.

### 3. Excitation of a smaller $Q$ component where $i_Q=1$

When  $L$  is larger, any change of the rotation energy during excitation is noticeable. Let us examine the  ${}^2F^e$  states. Evidently, the second state is excited by occupying the new components, which have  $i_Q=1$ . Since the first state has  $i=0$  for  $Q=2$ , the second state can occupy  $Q=0$  or 1, which has  $i=1$ . The  $Q=1$  component will be preferred since it has a smaller rotational energy in comparison with the  $Q=0$  component. Indeed the coefficients in Table V confirm this prediction. However, in comparison with the first state, which has  $i=0$  for  $Q=2$ , the second state has  $i=1$  for  $Q=1$ . Thus, in going from the first state to the second state not only is a nodal surface excited but also more rotational energy is excited since  $Q$  decreases from 2 to 1. We thus expect that the energy gap between the first two states in this case is also somewhat larger. From Table I we conclude that the first two states for  ${}^4G^o$  also belong to this type.

### 4. Excitation of a larger $Q$ component where $i_Q=1$

We also have situations analogous to Sec. IV F 3 but the  $Q$  for the second state is larger than for the first state. This occurs for the first two  ${}^2F^o$  states. The first state has  $i=0$  for  $Q=1$  and the second state can occupy  $i=1$  for  $Q=3$  and  $Q=2$ . The coefficients in Table V indeed confirm that these two components are large. In this case, we note that the second state acquires one inherent nodal surface, but its rotational energy is decreased. Thus the energy separation between the first and the second states will be smaller in comparison to the previous cases. From Table I we conclude that the first two states for  ${}^2G^o$ ,  ${}^4F^e$ ,  ${}^4H^e$ , and  ${}^4H^o$  belong to this type.

TABLE VI. Energy separation of the first two states for the  $3l3l'3l''$  states. The types of excitations are referred to in Sec. IV F. The results of  $\text{He}^-$  are from the  $r$ -frozen model and the results of  $\text{N}^{2+}$  are from a Hartree-Fock multiconfiguration calculation [9]. In both cases the energy separations of the first two  ${}^2P^o$  states are scaled as unity.

Type of excitation	${}^{2S+1}L^\pi$	$\text{He}^-$	$\text{N}^{2+}$
1	${}^2P^o$	1	1
	${}^4P^e$	1.60	1.24
2	${}^2F^e$	0.58	0.62
	${}^4F^o$	1.44	1.13
3	${}^2D^e$	0.68	0.43
	${}^2D^o$	0.56	0.41
4	${}^2F^o$	0.28	0.28
	${}^2G^o$	0.30	0.46
	${}^4F^e$	0.43	0.06
5	${}^2G^e$	0.55	0.45

### 5. Rotational excitation of a smaller $Q$ component where $i_Q=0$

Let us inspect states that have more than one free components. For the  ${}^2G^e$  symmetry, the first state will definitely occupy the free component with  $Q=4$  (refer to Table II). Since there is another free component that remains essentially empty, the second state can simply occupy this  $Q=2$  component. In this way, the internal structure (the coplanar equilateral triangle structure) remains unchanged, but the dominant  $Q$  has decreased, resulting in an increase of rotation energy. Thus the second state is a pure rotational excitation and this type is associated with an incline of the plane of the three electrons, from being perpendicular to the  $\vec{L}$  vector to being parallel. Evidently, since no internal excitation is involved, the energy separation in this type will be small.

So far, based on the inherent nodal structure, the excitations of all the second states containing the free components have been classified. The states without a free component can also be classified likewise, but will not be discussed here to avoid tedium.

Let us check the theoretical results of the energy separations as listed in Table VI. Here we normalize the energy separation between the two  ${}^2P^o$  states to unity. Clearly the separation for type 4 is significantly smaller than for the other cases. For the pure rotational excitation in  ${}^2G^e$ , there is a change of  $Q$  from 4 to 2 such that the energy separation between these two states is not quite small.

## V. SUMMARY AND FINAL REMARKS

In this paper we have studied in detail the inherent nodal structure of a three-electron system. By projecting the total wave function onto the body frame of the three electrons [Eq. (5)] where the body-frame quantization axis is chosen to be perpendicular to the plane of the three electrons, we analyzed the nodal structure of each of the rotational components and the following conclusions have been obtained.

(i) Since each wave function is required to have well-defined total orbital and spin angular momentum quantum numbers, well-defined parity, and permutation symmetry under electron exchange, these symmetry conditions impose

nodal surfaces on each of the rotational components of the wave functions. The existence of an inherent nodal surface implies that the wave function is forbidden at specific geometric symmetries and at the same time implies a specific oscillation about an equilibrium configuration. With respect to a coplanar equilateral triangle geometry where the plane of the three electrons coincides with the core, three basic modes of oscillations have been identified. They are the swing mode ( $s$ ) of the third electron with respect to the first two, the hinge mode ( $h$ ) of the first two electrons with respect to the third, or the  $d$ -oscillation mode where the plane of the three electrons moves up and down with respect to the core. There are some higher-order swing modes and combinations of these fundamental modes in each of the rotational components. Excitation of each of these modes implies higher energies.

(ii) Since the existence of nodal surfaces implies higher energies, the lower states belong to those symmetries that have rotational components that are free from any nodal surfaces, meaning that the basic  $s$ ,  $d$ , and  $h$  modes are not excited. These states can maintain the shape of a coplanar equilateral triangle, which has the lowest potential energy. They are further differentiated by the orientation of the plane with respect to the direction of the orbital angular momentum. This group of states have a nice rotor structure that is similar to that for a rigid rotor, as illustrated by Fig. 4.

(iii) The second group of states involves the excitation of one of the  $s$ ,  $h$ , and  $d$  modes (i.e.,  $i=1$ ). These states have higher energies. The next group belongs to states where new dynamic nodal surfaces are created (i.e.,  $v=1$ ). These often belong to the excited states of a given symmetry. By examining the nature of what kinds of modes are excited, the relative energy levels are explained. The numerical calculations are used to support qualitative interpretations that are based on the symmetry alone. In other words, the relative energy ordering of intrashell states for different symmetries revealed in the calculation or in actual atom are less affected by the specific Coulomb forces between the electrons, but more strongly affected by the symmetry condition. We have explored the relationship between the inherent symmetry and the relative energy levels to great details.

The inherent nodal structure affects not only the geomet-

ric character and the mode of internal oscillation of the first states, but also the ways of excitation adopted by the second states. Thus, by investigating the nature of the inherent nodal structure, a classification scheme for explaining the energy separation has been proposed. While the features of the wave functions obtained from the  $r$ -frozen model may be viewed as incomplete as far as the real atom is concerned, they would serve as a starting point for investigations where the radial degrees of freedom of the three electrons are taken into account. In this respect, we mention a complementary analysis [13] for three electrons where the angular degrees of freedom were frozen, but the radial degrees of freedom were analyzed. That analysis allowed us to conclude that singly excited states, doubly excited states, and triply excited states are distinguished by their nodal structures in the hyperangles

when the wave functions are examined in hyperspherical coordinates. One of the eventual goals of the study of three-electron atoms is to be able to analyze the nodal surfaces or “shapes” with both the radial and angular degrees of freedom included.

#### ACKNOWLEDGMENTS

This work was supported in part (C.G.B.) by the National Foundation of Natural Sciences of PRC, by a fund from the National Education Committee of the People’s Republic of China, and in part (C.D.L.) by the U.S. Department of Energy, Office of Basic Energy Sciences, Division of Chemical Sciences.

- 
- [1] C.D. Lin, in *Review of Fundamental Processes and Applications of Atoms and Ions*, edited by C. D. Lin (World Scientific, Singapore, 1993).
- [2] A. Menzel *et al.*, Phys. Rev. Lett. **75** 1479 (1995).
- [3] M. Domke *et al.*, Phys. Rev. A **53**, 1424 (1996).
- [4] Y. Azuma *et al.*, Phys. Rev. Lett. **74**, 3768 (1995).
- [5] L. M. Kiernan *et al.*, Phys. Rev. Lett. **72**, 2359 (1994); J. Phys. B **28**, L161 (1995).
- [6] L. Journal *et al.*, Phys. Rev. Lett. **76**, 30 (1996).
- [7] K.T. Chung and B.C. Gou, Phys. Rev. A **52**, 3669 (1995).
- [8] C.A. Nicolaidis, N.A. Piangos, and Y. Komninos, Phys. Rev. A **48**, 3578 (1993).
- [9] N. Vaeck and J.E. Hansen, J. Phys. B **25** 883 (1992).
- [10] Y. Komninos, M. Chrysos, and C.A. Nicolaidis, Phys. Rev. A **38**, 3182 (1988).
- [11] H. Bachau, J. Phys. B **29**, 4365 (1996).
- [12] C.G. Bao and C.D. Lin, Few Body Syst. **16**, 47 (1994).
- [13] Xiazhou Yang, C.G. Bao, and C.D. Lin, Phys. Rev. A **52**, 2029 (1995).
- [14] X. Yang *et al.*, Phys. Rev. Lett. **76**, 3096 (1996).
- [15] C.G. Bao, Few Body Syst. **13**, 41 (1992).
- [16] C.G. Bao, W.F. Xie, and C.D. Lin, J. Phys. B **27**, L193 (1994).
- [17] C.G. Bao, J. Phys. B **25**, 3725 (1992).
- [18] C.G. Bao and C.D. Lin, Phys. Rev. A **52**, 3586 (1995).
- [19] S. Watanabe and C.D. Lin, Phys. Rev. A **36**, 511 (1987).
- [20] C. E. Moore, *Atomic Energy Levels*, Natl. Bur. Stand. Ref. Data. Ser., Natl. Bur. Stand. (U.S.) Circ. No. 35 (U.S. GPO, Washington, DC, 1971).
- [21] C.D. Lin, Astrophys. J. **187**, 385 (1974).